

Investigating the Chemical Dynamics of the Reaction of Ground-State Carbon Atoms with Acetylene and Its Isotopomers

Xibin Gu, Ying Guo, Fangtong Zhang, and Ralf I. Kaiser*

Department of Chemistry, University of Hawai'i at Manoa, Honolulu, Hawaii 96822

Received: November 10, 2006; In Final Form: January 8, 2007

We investigated the multichannel reaction of ground-state carbon atoms with acetylene, C_2H_2 ($X^1\Sigma_g^+$), to form the linear and cyclic C_3H isomers (atomic hydrogen elimination pathway) as well as tricarbon plus molecular hydrogen. The experiments were conducted under single-collision conditions at three different collision energies between 8.0 kJ mol^{-1} and 31.0 kJ mol^{-1} . Our studies were complemented by crossed molecular beam experiments of carbon with three isotopomers C_2D_2 ($X^1\Sigma_g^+$), C_2HD ($X^1\Sigma^+$), and $^{13}C_2H_2$ ($X^1\Sigma_g^+$) to clarify a potential intersystem crossing (ISC), the effect of the symmetry of the reaction intermediates on the center-of-mass angular distributions, the collision energy-dependent branching ratios of the atomic versus molecular hydrogen elimination pathways, and deuterium-enrichment processes. The results are discussed in light of recent electronic structure and dynamics calculations.

1. Introduction

During the past decade, the reaction of ground-state carbon atoms, $C(^3P_1)$, with acetylene, C_2H_2 ($X^1\Sigma_g^+$), has received considerable interest both from experimental and theoretical viewpoints because of its importance in interstellar chemistry^{1–4} and in combustion processes.^{5–7} Pioneering kinetic studies suggested that the reaction of carbon atoms with acetylene is very fast in the temperature range of $293–15 \text{ K}$ ^{8,9} and proceeded with gas kinetics efficiency at rate constants of a few $10^{-10} \text{ cm}^3 \text{ s}^{-1}$. However, since these kinetic experiments only measured the disappearance of the initial atomic carbon reactant, complementary studies, which probe the nature of the reaction products, were imperative. The first crossed molecular beam experiments of carbon atoms with acetylene were carried out at collision energies between 8.8 and 45.0 kJ mol^{-1} . These studies verified the formation of C_3H isomers plus atomic hydrogen.^{10–12} On the basis of the center-of-mass angular distributions, the authors inferred the formation of cyclic (*c*- C_3H) and linear C_3H isomers (*l*- C_3H) via direct and indirect scattering dynamics, respectively. At lower collision energies, the cyclic isomer was suggested to be formed through a short-lived triplet cyclopropenylidene intermediate (**t2**) in a direct fashion, whereas the linear C_3H structure was synthesized via a propargylene intermediate **t4** (Figure 1).⁴ As the collision energy increased, the center-of-mass angular distributions became less forward scattering; this trend culminated in an isotropic (flat) distribution at a collision energy of 45.0 kJ mol^{-1} leading solely to the linear C_3H structure.

In combination with electronic structure calculations, the proposed chemical dynamics that caused an increasing ratio of *l*- C_3H to *c*- C_3H with rising collision energy could explain previously unresolved astronomical observations.¹² Dark molecular clouds hold typical averaged translational temperatures of 10 K , whereas circumstellar shells around carbon stars are heated up to about 4000 K ; this presents typical translational energies of about 0.1 and 40 kJ mol^{-1} , respectively. Therefore, both isomers are anticipated to exist in dark clouds, but less

c- C_3H in the hotter envelope surrounding the carbon star IRC+10216. This expected pattern is reflected in the observed number density ratios of *c*- C_3H versus *l*- C_3H . Five years later, the authors also detected the hitherto elusive molecular hydrogen elimination pathway leading to the tricarbon molecule, C_3 ($X^1\Sigma_g^+$).¹³ A subsequent study by Casavecchia et al. confirmed that the reaction of ground-state carbon atoms with acetylene opens up both the atomic and molecular hydrogen displacement pathways forming C_3H isomers and C_3 ($X^1\Sigma_g^+$), respectively.¹⁴ In this context, Mebel et al. predicted the formation of the tricarbon molecule to proceed via intersystem crossing (ISC) from triplet propargylene (**t4**) to singlet cyclopropenylidene (**s1**) followed by an atomic hydrogen migration to vinylidene carbene (**s2**) and a molecular hydrogen elimination process to tricarbon.¹⁵ Crossed beam experiments conducted at collision energies as low as 4 meV utilizing D2-acetylene and atomic carbon demonstrated explicitly that this reaction has no entrance barrier.¹⁶ In addition, however, the determination of the hydrogen atom production rate of only about $53 \pm 4\%$ at room temperature confirmed Kaiser et al.'s and Casavecchia et al.'s conclusions that a second reaction channel, besides the atomic carbon versus hydrogen exchange pathway, must be involved.¹⁷

In addition to kinetics and dynamics studies, computational investigations of the reaction of carbon atoms with acetylene have been conducted at various levels of theory.¹⁸ The majority of the calculations suggest that the cyclic C_3H isomer is lower in energy by about $4–8 \text{ kJ mol}^{-1}$ than the linear isomer. Buonomo and Clary conducted a quantum study on the reaction of ground-state carbon atoms with acetylene utilizing a reduced dimensionality approach in the range covering collision energies from 5 kJ mol^{-1} to 70 kJ mol^{-1} .¹⁹ The authors concluded that *l*- C_3H is preferentially formed, while the cyclic structure is only obtained at the highest collision energies. On the other hand, Takayanagi reported quantum calculations of the reaction cross section.²⁰ These studies yielded branching ratios favoring the cyclic C_3H isomer at all collision energies. The most recent computational investigation by Park et al. spanned collision energies from 5 kJ mol^{-1} to 40 kJ mol^{-1} and tackled both the

* To whom correspondence should be addressed.

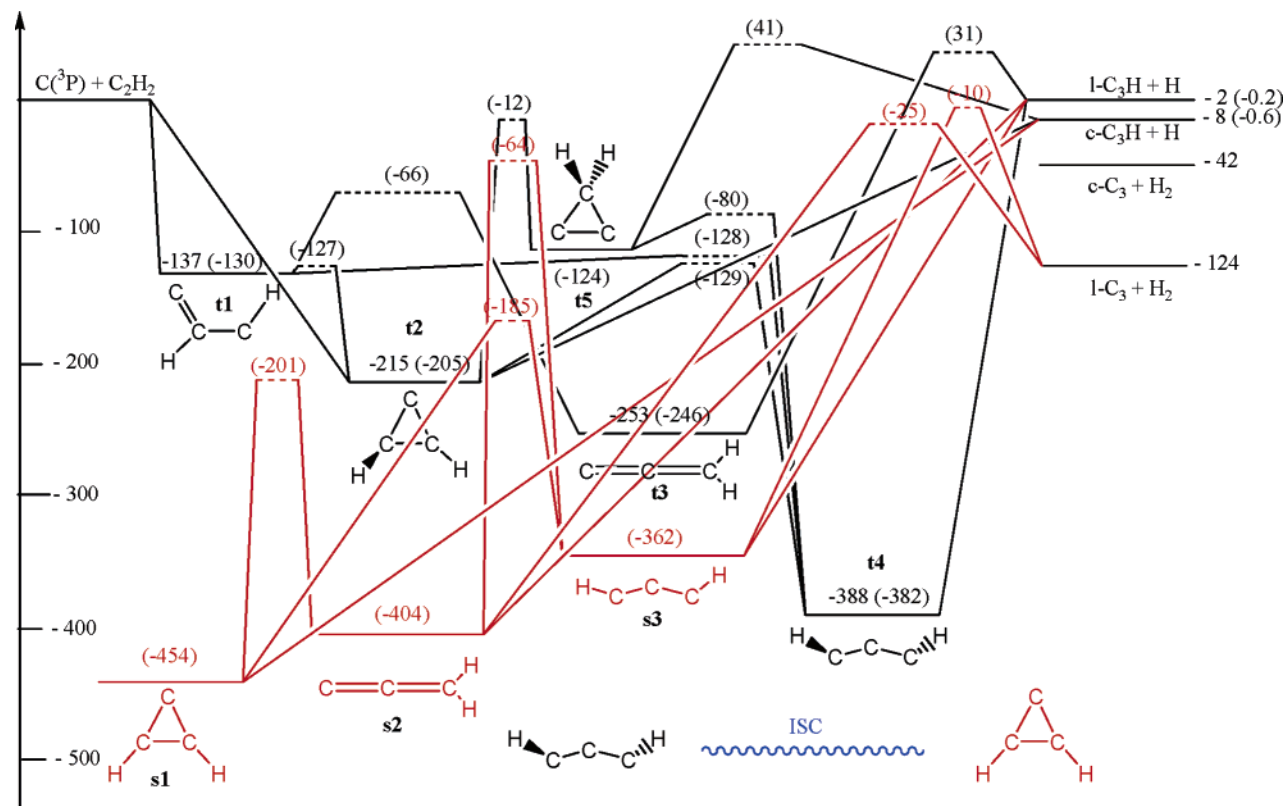


Figure 1. Schematic representation of the triplet and singlet C_3H_2 potential energy surfaces (PES). Relative energies are given in units of kJ mol^{-1} as compiled from Ochsenfeld et al. (1996); numbers in parenthesis are taken from Bowman et al. (2006). Black: triplet surface; red: singlet surface.

triplet and singlet C_3H_2 surfaces.²¹ Their trajectory calculations suggested that linear C_3H should dominate over the cyclic isomer at all collision energies on the triplet surface. This finding is in strong contrast to Takayanagi, possibly because one entrance channel in which atomic carbon adds to the carbon-carbon triple bond of the acetylenic molecule forming triplet cyclopropenylidene (**t2**) followed by ring opening was not considered. On the singlet surface, Park et al. predicted the linear and cyclic C_3H as well as the molecular hydrogen elimination channel to tricarbon to be formed in almost equal amounts.²¹

These discrepancies make it clear that several aspects of this reaction have remained unanswered so far. Although Mebel et al.'s calculations predict that triplet propargylene (**t4**) is the central intermediate in ISC to the singlet surface, neither laboratory nor computational studies were able to elucidate if triplet propargylene (**t4**) is formed via (1) addition of $C(^3P_j)$ to one carbon atom of acetylene forming **t1** followed by a hydrogen migration, (2) via **t1** followed by ring closure to **t2** and consecutive ring opening, or (3) via addition of $C(^3P_j)$ to two carbon atoms of acetylene yielding **t2** followed by ring opening; recall that all three microchannels have similar barriers (Figure 1). Second, it is important to pin down to what extent the lifetime of **s2** influences the molecular hydrogen elimination pathway. Third, an answer is desired whether the forward-backward symmetry of the center-of-mass angular distribution of the microchannel leading, from triplet propargylene (**t4**), to l - C_3H is the result of a long-lived triplet propargylene intermediate or solely an artifact of the C_2 symmetry of intermediate ("symmetric" intermediate). Recall that a symmetric intermediate is classified as a decomposing complex in which a leaving hydrogen atom can be interconverted by a 2-fold rotation axis. This would give an equal probability that the hydrogen atom is leaving in a direction of θ° or $\pi - \theta^\circ$; as a result, the center-

of-mass angular distribution is forward-backward symmetric although the lifetime of the intermediate might be less than its rotation period.¹² Finally, it is crucial to supply collision-energy branching ratios of the atomic versus molecular hydrogen loss pathways. This would enable a direct comparison between the experiments and the theoretically predicted branching ratios once intersystem crossing rate constants become available.

To shed a light on these open questions, we expanded our previous studies on the reaction of ground-state carbon atoms with acetylene¹⁰⁻¹² and examined the collision-energy-dependent chemical dynamics of the reaction between ground-state carbon atoms, $C(^3P_j)$, with acetylene, C_2H_2 ($X^1\Sigma_g^+$), at three collision energies between 8.0 kJ mol^{-1} and 30.7 kJ mol^{-1} utilizing pulsed supersonic beams of carbon and acetylene. Recall that our previous studies employed pulsed carbon but continuous acetylene beams. Therefore, these experiments serve as a cross check that the timing sequence in the pulsed experiments is correct (in an ideal case, both sets of experiments should yield identical center-of-mass translational and angular distributions). These studies also help to determine collision-energy-dependent branching ratios between the atomic and molecular hydrogen loss pathways and provide information on the energy-dependent dynamics of the molecular hydrogen elimination channel. In addition, we carried out the reaction with isotopically labeled $^{13}C_2H_2$ ($X^1\Sigma_g^+$), C_2D_2 ($X^1\Sigma_g^+$), and C_2HD ($X^1\Sigma^+$) at similar collision energies as the acetylene reactant. Here, the reaction of ground-state carbon atoms with the C_2HD ($X^1\Sigma^+$) reactant would lead to a triplet D1-propargylene intermediate. This effectively reduces the symmetry from C_2 in triplet propargylene to C_1 in the corresponding D1-propargylene intermediate thus eliminating the 2-fold rotational axis. Therefore, the D1-acetylene experiments are expected to help elucidate to what extent the forward-backward symmetric center-of-mass angular

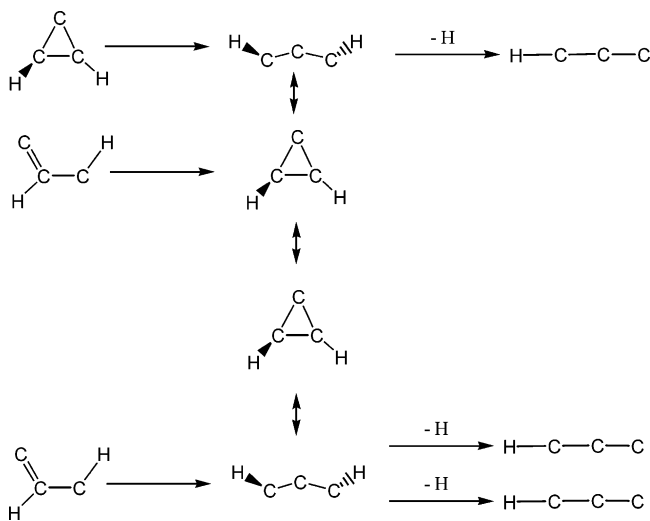


Figure 2. Schematic representation of three distinct reaction pathways in the reaction of carbon atoms, $C(^3P_j)$, with $^{13}C_2$ -acetylene, $^{13}C_2H_2$ ($X^1\Sigma_g^+$), to form various isotopomers of the 1- C_3H isomer. The attacking ^{12}C atom is denoted in blue.

distribution of the microchannel originating from triplet propargylene is the effect of the symmetry of the intermediate or truly from a long-lived propargylene complex behavior. In addition, by probing the atomic hydrogen atomic deuterium elimination pathways and the inherent formation of C_3D versus C_3H isomers, we will yield valuable information on potential isotopic effects. Finally, we carried out experiments with $^{13}C_2H_2$ ($X^1\Sigma_g^+$). Here, the reaction of $^{12}C(^3P_j)$ with $^{13}C_2H_2(X^1\Sigma_g^+)$ could yield two distinctive isotopomers of triplet propargylene: $H-^{12}C-^{13}C-^{13}C-H$ (C_1 symmetry) and $H-^{13}C-^{12}C-^{13}C-H$ (C_2 symmetry) (Figure 2). Consequently, the involvement of different isotopomers could result in changes of the center-of-mass angular distributions on the basis of a switch from a symmetric to a nonsymmetric reaction intermediate.

2. Experimental Setup and Data Processing

The experiments were conducted under single-collision conditions in a crossed molecular beam machine at The University of Hawaii.²² Briefly, the main chamber is evacuated to the low 10^{-8} Torr region. Both source chambers are placed inside the main chamber so that the reactant beams cross perpendicularly. Pulsed carbon beams were produced in the primary source by laser ablation of graphite at 266 nm by tightly focusing 10–20 mJ per pulse at 30 Hz on the rotating carbon rod.²³ The ablated species were seeded in neat carrier gas (helium or neon, 99.9999%, 3040 Torr, Table 1) released by a Proch-Trickl pulsed valve. After passing a skimmer, a four-slot chopper wheel mounted after the ablation zone selected a part out of the seeded carbon beam which then crossed a pulsed acetylene beam (C_2H_2 ; 99.99% after removal of the acetone stabilizer via a zeolitic trap and acetone–dry ice cold bath) under a well-defined collision energy in the interaction region (Table 1). The acetylene beam was also replaced by beams of isotopically labeled $^{13}C_2H_2(X^1\Sigma_g^+)$, $C_2HD(X^1\Sigma^+)$, and $C_2D_2(X^1\Sigma_g^+)$ (Cambridge Isotopes; 99.8–99.9%). At all velocities, the ablation beams contain also dicarbon and tricarbon molecules. However, since the dynamics of dicarbon with acetylene and their isotopomers is well established,²⁴ we can discriminate to what extent the scattering signal originates from the reaction with dicarbon or atomic carbon. Tricarbon reacts with acetylene only at collision energies larger than about 85 kJ mol^{-1} , well above our highest collision energy of 31.0 kJ mol^{-1} .²⁵ The

TABLE 1: Peak Velocities (v_p), Speed Ratios (S), and Center-of-Mass Angles (Θ_{CM}) Together with the Nominal Collision Energies of the Dicarbon and the Acetylene Reactants (E_c)

beam	v_p, ms^{-1}	S	$E_c, \text{kJ mol}^{-1}$	Θ_{CM}
$C_2H_2(X^1\Sigma_g^+)$	903 ± 3	16.0 ± 0.3		
$C(^3P)/Ne$	1063 ± 10	4.90 ± 0.33	8.0 ± 0.1	61.5 ± 0.3
$C(^3P)/He$	2037 ± 25	4.91 ± 0.20	20.4 ± 0.4	43.8 ± 0.4
$C(^3P)/He$	2581 ± 28	2.94 ± 0.12	30.7 ± 0.6	37.2 ± 0.4
$^{13}C_2H_2(X^1\Sigma_g^+)$	890 ± 5	16.0 ± 0.3		
$C(^3P)/Ne$	1057 ± 21	5.03 ± 0.29	8.0 ± 0.2	63.0 ± 0.6
$C(^3P)/He$	1950 ± 18	4.44 ± 0.14	19.3 ± 0.3	46.8 ± 0.4
$C(^3P)/He$	2537 ± 39	3.30 ± 0.14	30.4 ± 0.9	39.3 ± 0.6
$C_2D_2(X^1\Sigma_g^+)$	890 ± 5	16.0 ± 0.3		
$C(^3P)/Ne$	1059 ± 12	4.92 ± 0.25	8.0 ± 0.1	63.0 ± 0.4
$C(^3P)/He$	1978 ± 14	5.13 ± 0.23	19.8 ± 0.3	46.4 ± 0.4
$C(^3P)/He$	2566 ± 37	3.33 ± 0.13	31.0 ± 0.8	39.0 ± 0.6
$C_2HD(X^1\Sigma^+)$	890 ± 5	16.0 ± 0.3		
$C(^3P)/Ne$	1080 ± 10	5.11 ± 0.31	8.1 ± 0.1	61.7 ± 0.4
$C(^3P)/He$	1976 ± 17	5.30 ± 0.17	19.5 ± 0.3	45.4 ± 0.4
$C(^3P)/He$	2566 ± 45	3.19 ± 0.17	30.6 ± 1.0	38.0 ± 0.7

reactively scattered species were monitored using a triply differentially pumped quadrupole mass spectrometric detector (QMS) in the time-of-flight (TOF) mode after electron-impact ionization of the neutral molecules. Our detector can be rotated within the plane defined by the primary and the secondary reactant beams to allow taking angular-resolved TOF spectra. By taking and integrating the TOF spectra, we obtain the laboratory angular distribution, that is, the integrated signal intensity of an ion of distinct m/z versus the laboratory angle. Information on the chemical dynamics were obtained by fitting these TOF spectra of the reactively scattered products and the product angular distribution in the laboratory frame (LAB) using a forward-convolution routine which is described in detail in refs 26 and 27. This procedure assumes an angular distribution $T(\theta)$ and a translational energy distribution $P(E_T)$ in the center-of-mass reference frame (CM). TOF spectra and the laboratory angular distribution were then calculated from these $T(\theta)$ and $P(E_T)$ taking into account the beam spreads and the apparatus functions. Best fits of the TOF and laboratory angular distributions were achieved by refining the $T(\theta)$ and $P(E_T)$ parameters.

3. Results

3.1. Laboratory Data. *3.1.1. The $C(^3P_j)/C_2H_2$ System.* We scanned for reactive scattering signal at mass-to-charge ratios of $m/z = 37$ (C_3H^+) and 36 (C_3^+) at all three collision energies. Selected TOF spectra and the resulting laboratory angular distributions are shown in Figures 3a and 4a, respectively. At the forward angles with respect to the ablation beam, signal had to be fit with two contributions, that is, dissociative electron impact ionization of the C_4H product formed in the reaction of dicarbon with acetylene and the ionized reaction product of the carbon versus atomic hydrogen exchange channel, C_3H^+ . At larger angles, reactive scattering signal at $m/z = 37$ originated solely from the reaction of carbon atoms with acetylene. At $m/z = 36$, multiple channels were necessary to fit the data. These are from fragmentation of C_4H^+ to C_3^+ , fragmentation of C_3H^+ to C_3^+ , the ionized C_3 reaction product from the reaction of atomic carbon with acetylene, and inelastically scattered tricarbon. As we moved to angles closer to the secondary beam, that is, TOF spectra taken at laboratory angles of 65.0° ($E_c = 8.0 \text{ kJ mol}^{-1}$), 48.5° ($E_c = 20.4 \text{ kJ mol}^{-1}$), and 52.5° ($E_c = 30.7 \text{ kJ mol}^{-1}$), only two channels were necessary to adequately fit the TOF data and the LAB distributions. These are fragmentation of C_3H^+ to C_3^+ (slow component) and the ionized C_3 reaction

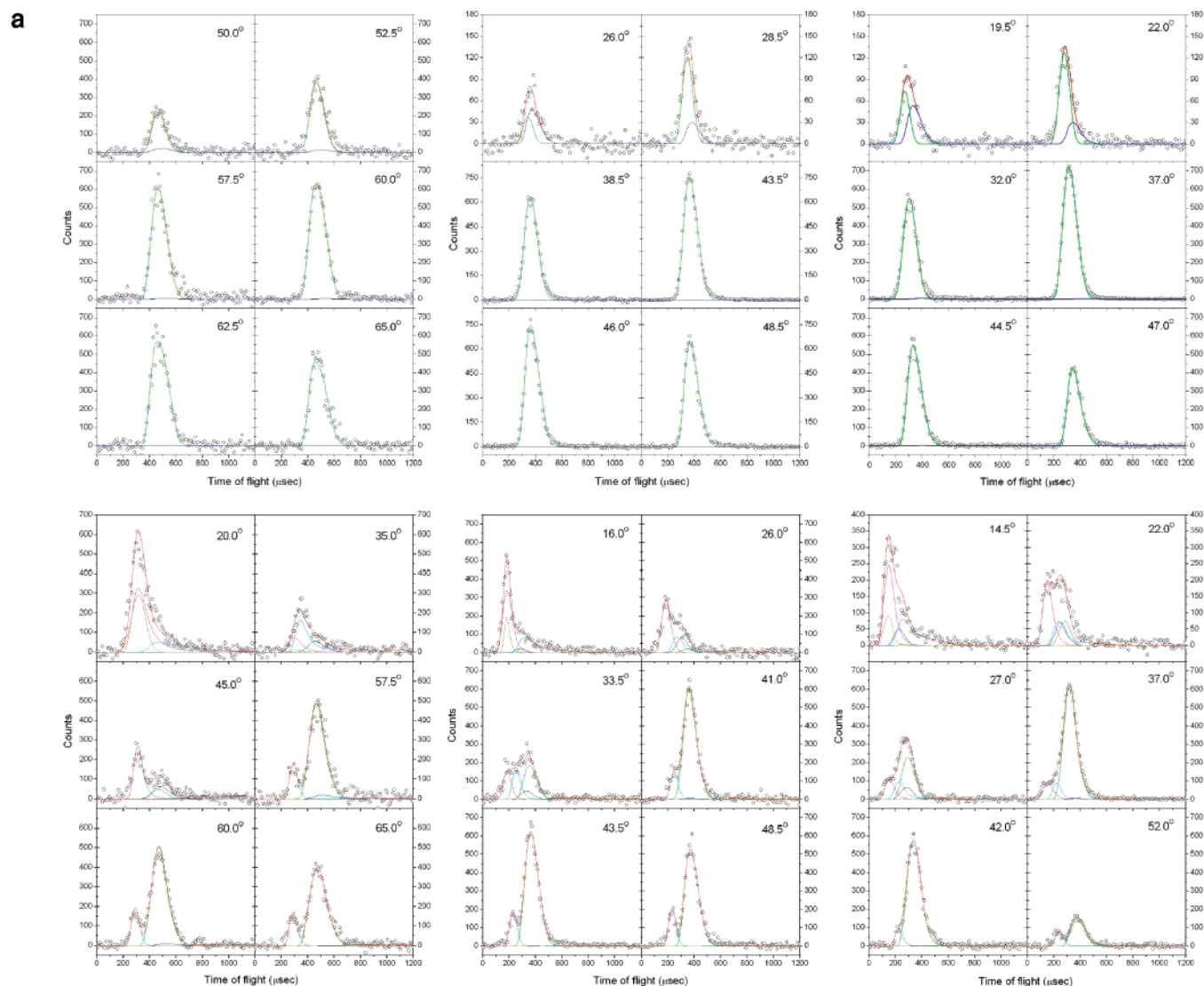


Figure 3. Part 1 of 4.

product from the reaction of atomic carbon with acetylene (fast component). Both contributions can be clearly separated in the TOF spectra.

3.1.2. The $C(^3P_j)/^{13}C_2H_2$ System. Considering the $^{13}C_2H_2$ reactant, we recorded TOF spectra at mass-to-charge ratios of $m/z = 39$ ($^{12}C^{13}C_2H^+$) and $m/z = 38$ ($^{12}C^{13}C_2^+$) together with the corresponding laboratory angular distributions (Figures 3b and 4b). Similar to the acetylene system (3.1.1.), the TOFs of $m/z = 39$ at angles close to the primary beam had to be fit with two contributions, that is, signal from dissociative electron impact ionization of the $^{13}C_2^{12}C_2H$ product formed in the reaction of dicarbon with $^{13}C_2H_2$ and the ionized reaction product of the carbon versus atomic hydrogen exchange channel, $^{13}C_2^{12}CH^+$. At larger angles, reactive scattering signal at $m/z = 39$ originated only from the reaction of carbon atoms with $^{13}C_2H_2$ (Figures 3b and 4b). The advantage of the $^{13}C_2H_2$ reactant is to probe the molecular hydrogen elimination channel at $m/z = 38$ ($^{12}C^{13}C_2^+$) without contamination from inelastically scattered tricarbon from the ablation beam which gives only signal at $m/z = 36$ ($^{12}C_3^+$). In case of $m/z = 38$, we have clearly eliminated the contributions from elastically scattered tricarbon as evident from Figures 3b and 4b. The TOFs at $m/z = 38$ need to be fit only with three channels, that is, dissociative ionization of the $^{13}C_2^{12}C_2H$ (channel 1) and $^{13}C_2^{12}CH$ products (channel

2) formed via reaction of dicarbon and carbon atoms with $^{13}C_2H_2$, respectively, and the molecular hydrogen elimination pathway to form $^{13}C_2^{12}C$ (channel 3).

3.1.3. The $C(^3P_j)/C_2D_2$ System. The TOF spectra recorded in the reaction of ground-state carbon atoms, $C(^3P_j)$, with D2-acetylene, $C_2D_2(X^1\Sigma_g^+)$, are shown together with the laboratory distributions for $m/z = 38$ (C_3D^+) and $m/z = 36$ (C_3^+) in Figures 3c and 4c. At $m/z = 38$, the TOFs had to be fit with two contributions from dissociative ionization of the C_4D reaction product of the dicarbon plus D2-acetylene reaction to C_3D^+ and also from the ionized C_3D product formed in bimolecular collisions of carbon atoms with D2-acetylene. Data at $m/z = 36$ originate from dissociative ionization of the C_4D and C_3D products (see above); in addition, signal arises from the molecular deuterium elimination pathway to form tricarbon and also from inelastically scattered tricarbon molecules present in the primary beam.

3.1.4. The $C(^3P_j)/C_2HD$ System. In case of D1-acetylene (C_2HD), the atomic hydrogen and deuterium loss pathways were monitored at $m/z = 38$ (C_3D^+) and $m/z = 37$ (C_3H^+). Figures 3d and 4d compile the TOF spectra for the atomic hydrogen/deuterium loss channels and the derived laboratory angular distributions, respectively. As expected, two channel fits were imperative for TOFs at both $m/z = 38$ and 37. These channels

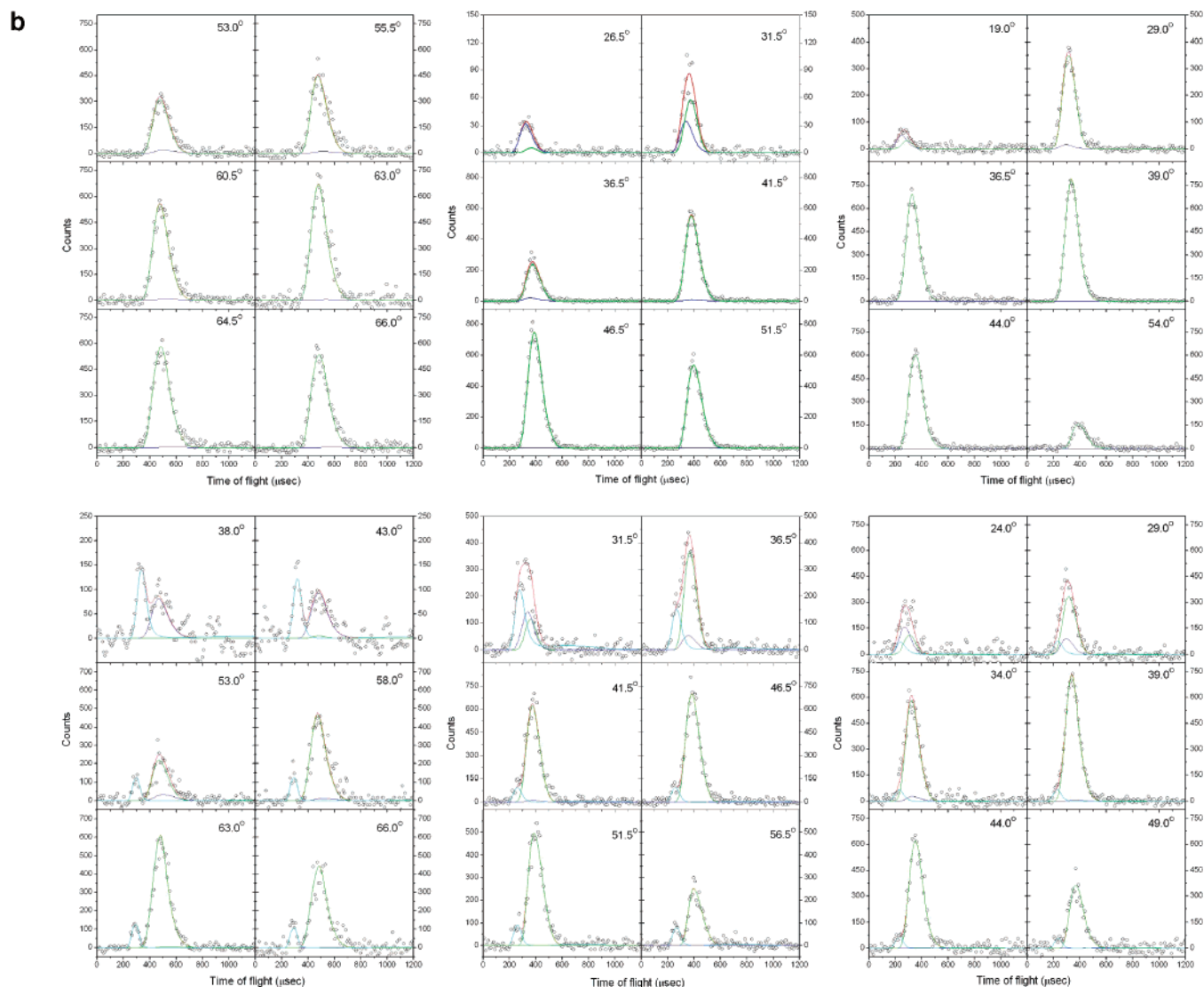


Figure 3. Part 2 of 4.

involved the dissociative ionization of the C_4H/C_4D product of the dicarbon plus D1-acetylene reaction to give C_3D^+ and C_3H^+ ions and also the ionized C_3D and C_3H products of the carbon plus D1-acetylene reaction at $m/z = 38$ and 37 , respectively. The multichannel fits of the reactive scattering signal at $m/z = 36$ are very tricky. Four channels are necessary to account for the signal from dissociative ionization of the C_4H/C_4D as well as C_3H/C_3D products. One channel accounts for the tricarbon plus HD pathway; the contribution from inelastically scattered tricarbon is included, too (Figures 3d and 4d).

3.2. Center-of-Mass Functions. Figure 5 presents the translational energy distributions in the center-of-mass-frame, $P(E_T)$, together with the center-of-mass angular distributions, $T(\theta)$, for the atomic hydrogen/deuterium loss (upper row) and the molecular hydrogen/deuterium/deuteriumhydride elimination channels (lower row). As the collision energy increases, the shape of the derived $T(\theta)$ functions changes dramatically. Considering the atomic hydrogen/deuterium loss pathway to form C_3H/C_3D isomers, the center-of-mass angular distributions become less forward scattered as the collision energy increases. Our fitting route suggests intensity ratios at the poles, $T(0^\circ)/T(180^\circ)$, decreasing from 2.1 ± 0.1 via 1.4 ± 0.1 to 1.2 ± 0.1 as the collision energy rises. This correlated nicely with an early study of this system which was conducted with pulsed carbon

and continuous acetylene beams suggesting that at least two microchannels are involved in the formation of the tricarbon hydride molecules together with their isotopomers.¹¹ This finding clearly indicates that the delay timing sequence of the present experiments conducted solely under pulsed conditions is correct. Also, within the error limits, the atomic hydrogen/deuterium elimination pathways in the $C(^3P_j)C_2H_2(X^1\Sigma_g^+)$, $C(^3P_j)^{13}C_2H_2(X^1\Sigma_g^+)$, $C(^3P_j)C_2HD(X^1\Sigma^+)$, and $C(^3P_j)_2D_2(X^1\Sigma_g^+)$ systems could all be fit, at similar collision energies, with identical center-of-mass functions. Finally, best fits of the TOF spectra and the LAB distributions were achieved at each collision energy with a single $P(E_T)$ extending to maximum translational energies E_{max} , of about 20 ± 5 kJ mol⁻¹ ($E_c = 8.0\text{--}8.1$ kJ mol⁻¹), 33 ± 5 kJ mol⁻¹ ($E_c = 19.3\text{--}20.4$ kJ mol⁻¹), and 44 ± 5 kJ mol⁻¹ ($E_c = 30.4\text{--}31.0$ kJ mol⁻¹). Since the maximum translational energy reflects the sum of the collision energy and the absolute of the exoergicity of the reaction, the magnitude of E_{max} can be utilized to compute the reaction exoergicity. Here, we find that the reactions to form tricarbon hydride plus atomic hydrogen/deuterium is exoergic by 20 ± 5 kJ mol⁻¹. Assuming that only the energetically most stable, cyclic isomer is formed, we can also compute the fraction of available energy channeling into the translational degrees of the

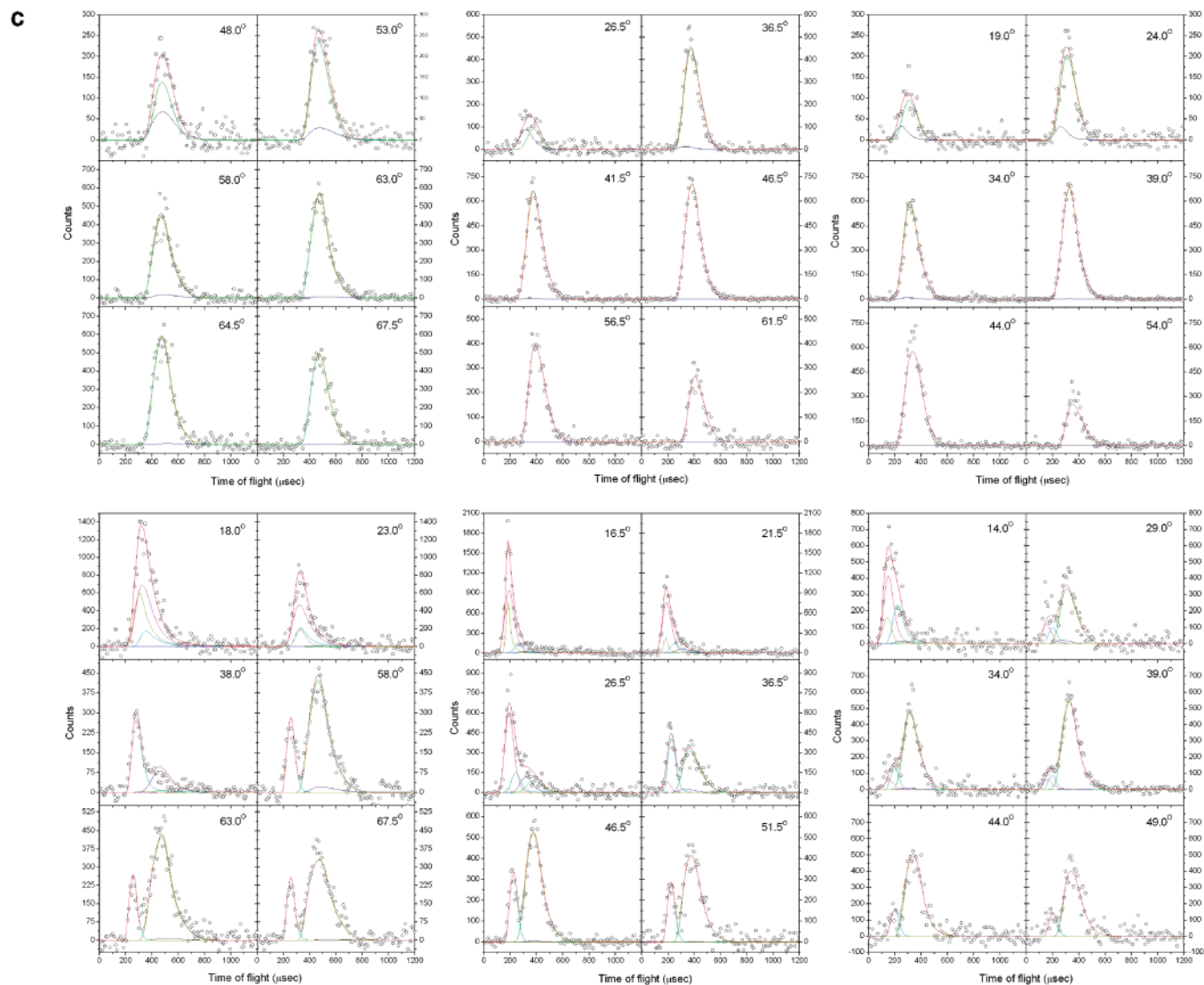


Figure 3. Part 3 of 4.

reaction products to be about $38 \pm 5\%$ almost invariant on the collision energy.

In case of the tricarbon plus molecular hydrogen/deuterium/deuteriumhydride elimination channels, we find that as the collision energy rises, the $T(\theta)$ becomes increasingly forward scattered. This finding indicates the existence of a reaction intermediate whose lifetime decreases as the collision energy is raised from 8.0 to 31.0 kJ mol^{-1} , that is, a classical “osculating” complex model.²⁸ Quantitatively, we find that the intensity ratios at the poles, $T(0^\circ)/T(180^\circ)$, increase from 1.9 ± 0.2 via 3.1 ± 0.4 to 9.0 ± 3.3 . Also, the intensity over the complete angular range from 0° to 180° is indicative of an indirect reaction mechanism; the asymmetry relates to a complex lifetime which is less than its rotational period.²⁸ Also, the $P(E_T)$ s extend to translational energies of up to 115 ± 4 kJ mol^{-1} ($E_c = 8.0\text{--}8.1$ kJ mol^{-1}), 127 ± 5 kJ mol^{-1} ($E_c = 19.3\text{--}20.4$ kJ mol^{-1}), and 137 ± 5 kJ mol^{-1} ($E_c = 30.4\text{--}31.0$ kJ mol^{-1}). This suggests a reaction exoergicity of 107 ± 4 kJ mol^{-1} in excellent agreement with the NIST data of 104 kJ mol^{-1} . Compared to the atomic hydrogen/deuterium elimination pathway, the pronounced peaking of the $P(E_T)$ s far away from zero translational energy is the most striking difference. Here, distribution maxima are in the range of 85 , 100 , and 110 kJ mol^{-1} as the collision energy rises. This “off-zero” peaking

likely indicates a significant exit barrier and an inherent tight exit transition state from the decomposing complex to form tricarbon plus molecular hydrogen/deuterium/deuterium hydride.²⁹ Similar to the atomic hydrogen/deuterium loss pathways, the center-of-mass functions of the tricarbon channel were for each range of collision energies identical for all isotopomers. Finally, the fraction of available energy channeling into the translational degrees of the reaction products was about $66 \pm 6\%$ independent of the collision energy.

3.3. Branching Ratios. In case of multichannel reactions, crossed beam experiments can be utilized to extract the branching ratios, R , of the pathways involved. Considering a two-channel reaction, the branching ratio between channel A (the atomic hydrogen loss pathway) and channel B (the molecular hydrogen loss pathway) having cross sections σ_{C_3H} and σ_{C_3} , computes via eq 1.³⁰

$$R = \frac{\sigma_{C_3H}}{\sigma_{C_3}} = \frac{\sigma_{C_3H}^0 Q_{C_3} F_{C_3C_3+}}{\sigma_{C_3}^0 Q_{C_3H} F_{C_3HC_3+}} \quad (1)$$

Here, $\sigma_{C_3H}^0/\sigma_{C_3}^0$ is the apparent branching ratio and is given by the output of the fitting routine described in refs 26 and 27 to fit the TOF spectra of $m/z = 36$ (C_3^+); Q_{C_3} and Q_{C_3H} are the

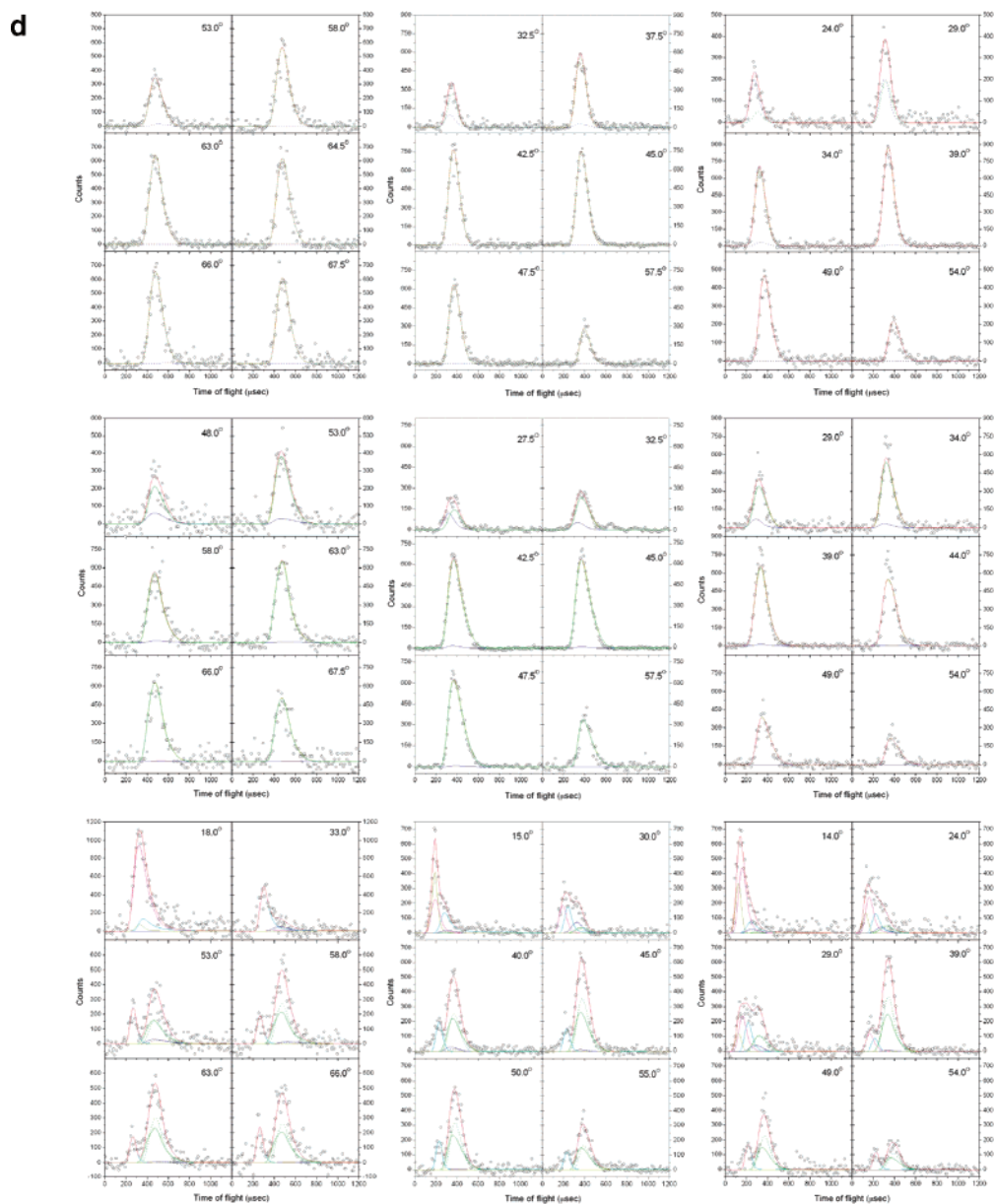


Figure 3. Part 4 of 4. (a) Time-of-flight (TOF) spectra recorded in the reaction of ground-state carbon atoms, $C(^3P_j)$, with acetylene, $C_2H_2(X^1\Sigma_g^+)$, at $m/z = 37$ (C_3H^+) (upper row) and $m/z = 36$ (C_3^+) (lower row) for three collision energies at 8.0 kJ mol^{-1} (left column), 20.4 kJ mol^{-1} (central column), and 30.7 kJ mol^{-1} (right column). Color code $m/z = 37$: dark blue (fragmentation of C_4H^+ to C_3H^+), light green (ionized C_3H reaction product, C_3H^+). Color code $m/z = 36$: dark blue (fragmentation of C_4H^+ to C_3^+), light green (fragmentation of C_3H^+ to C_3^+), light blue (ionized C_3 reaction product, C_3^+), pink (ionized inelastically scattered C_3 , C_3^+). (b) TOF spectra recorded in the reaction of ground-state carbon atoms, $C(^3P_j)$, with $^{13}C_2$ -acetylene, $^{13}C_2H_2(X^1\Sigma_g^+)$ at $m/z = 39$ ($^{12}C^{13}C_2H^+$) (upper row), and $m/z = 38$ ($^{12}C^{13}C_2^+$) (lower row) for three collision energies at 8.0 (left column), 19.3 (central column), and 30.4 kJ mol^{-1} (right column). Color code $m/z = 39$: dark blue (fragmentation of $^{12}C_2^{13}C_2H^+$ to $^{12}C^{13}C_2H^+$), light green (ionized $^{12}C^{13}C_2H$ reaction product, $^{12}C^{13}C_2H^+$). Color code $m/z = 38$: dark blue (fragmentation of $^{12}C_2^{13}C_2H^+$ to C_3^+), light green (fragmentation of $^{12}C^{13}C_2H^+$ to $^{12}C^{13}C_2^+$), light blue (ionized $^{12}C^{13}C_2$ reaction product, $^{12}C^{13}C_2^+$). (c) TOF spectra recorded in the reaction of ground-state carbon atoms, $C(^3P_j)$, with D2-acetylene, $C_2D_2(X^1\Sigma_g^+)$, at $m/z = 38$ (C_3D^+) (upper row) and $m/z = 36$ (C_3^+) (lower row) for three collision energies at 8.0 (left column), 19.8 (central column), and 31.0 kJ mol^{-1} (right column). Color code $m/z = 38$: dark blue (fragmentation of C_4D^+ to C_3D^+), light green (ionized C_3D reaction product, C_3D^+). Color code $m/z = 36$: dark blue (fragmentation of C_4D^+ to C_3^+), light green (fragmentation of C_3D^+ to C_3^+), light blue (ionized C_3 reaction product, C_3^+), pink (ionized inelastically scattered C_3 , C_3^+). (d) TOF spectra recorded in the reaction of ground-state carbon atoms, $C(^3P_j)$, with D1-acetylene, $C_2HD(X^1\Sigma^+)$, at $m/z = 38$ (C_3D^+) (upper row), $m/z = 37$ (C_3H^+) (central row), and $m/z = 36$ (C_3^+) (lower row) for three collision energies at 8.1 (left column), 19.5 (central column), and 30.6 kJ mol^{-1} (right column). Color code $m/z = 38$: dark dashed blue (fragmentation of C_4D^+ to C_3D^+), light dashed green (ionized C_3D reaction product, C_3D^+). Color code $m/z = 37$: dark blue (fragmentation of C_4H^+ to C_3H^+), light green (ionized C_3H reaction product, C_3H^+). Color code $m/z = 36$: dark blue (fragmentation of C_4H^+ to C_3^+), dark dashed blue (fragmentation of C_4D^+ to C_3^+), light green (fragmentation of C_3D^+ to C_3^+), light dashed green (fragmentation of C_3H^+ to C_3^+), light blue (ionized C_3 reaction product, C_3^+), pink (ionized inelastically scattered C_3 , C_3^+).

total ionization cross sections, $^{30} F_{C_3H,C_3^+}$ is the fraction of the ion signal detected at $m/z = 36$ for the C_3H neutral, and F_{C_3,C_3^+} is the fraction of the ion signal detected at $m/z = 36$ for the C_3

neutral. This treatment assumes that masses lower than $m/z = 36$ are not taken into account and that the transmission of $m/z = 37$ and 36 is identical. Equation 1 can be utilized now to

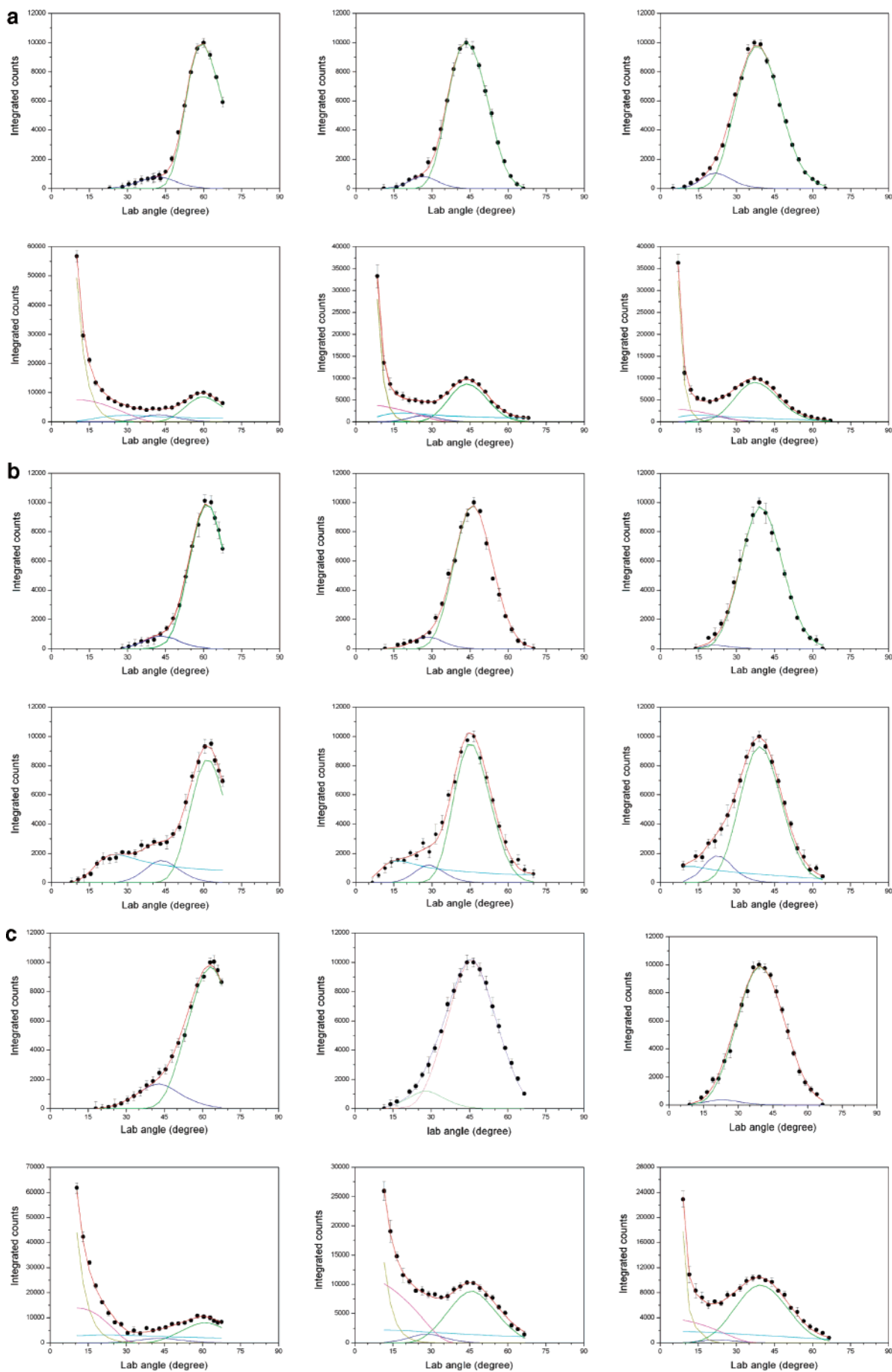


Figure 4. Part 1 of 2.

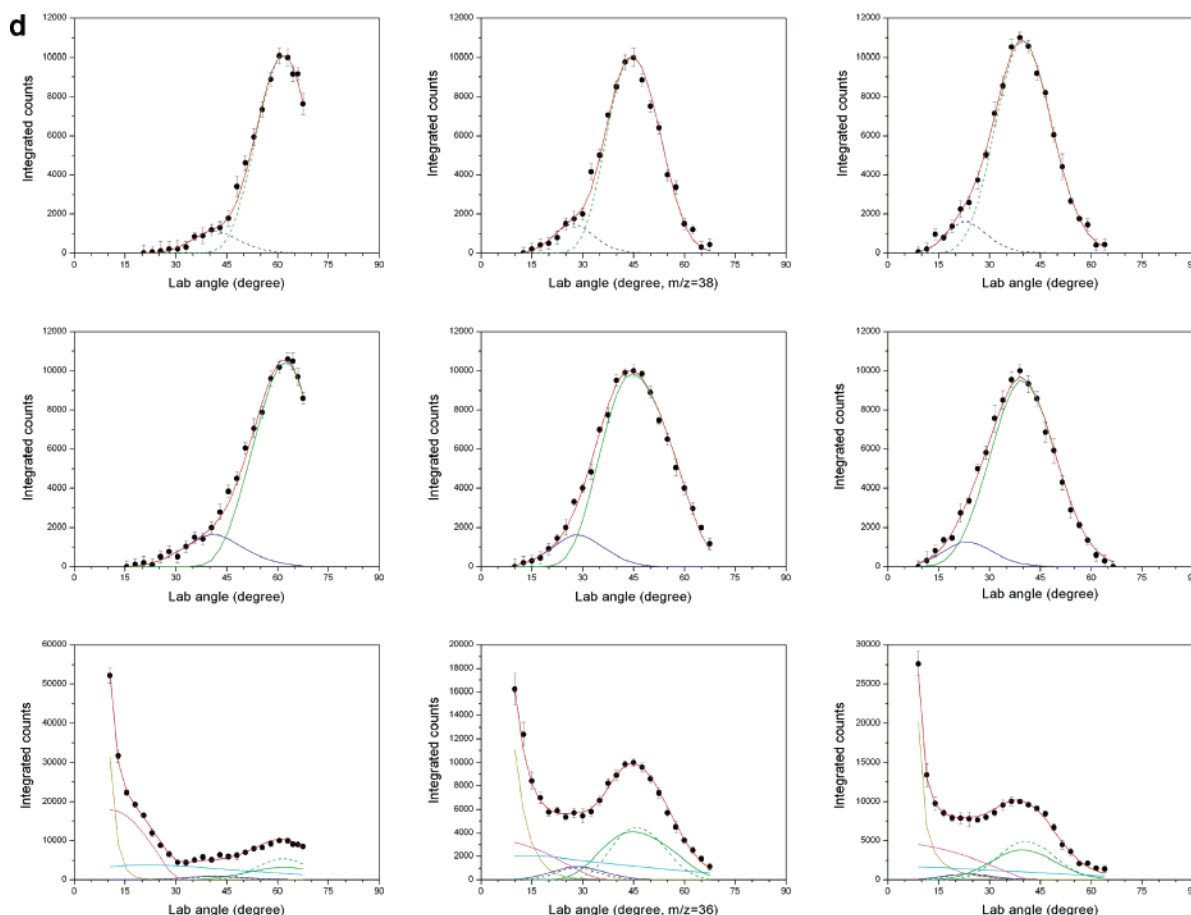


Figure 4. Part 2 of 2. (a) LAB distributions recorded in the reaction of ground-state carbon atoms, $C(^3P_j)$, with acetylene, $C_2H_2(X^1\Sigma_g^+)$, at $m/z = 37$ (C_3H^+) (upper row) and $m/z = 36$ (C_3^+) (lower row) for three collision energies at 8.0 (left column), 20.4 (central column), and 30.7 kJ mol^{-1} (right column). The color code is defined in Figure 3a. (b) LAB distributions recorded in the reaction of ground-state carbon atoms, $C(^3P_j)$, with $^{13}C_2$ -acetylene, $^{13}C_2H_2(X^1\Sigma_g^+)$, at $m/z = 39$ ($^{12}C^{13}C_2H^+$) (upper row) and $m/z = 38$ ($^{12}C^{13}C_2^+$) (lower row) for three collision energies at 8.0 (left column), 19.3 (central column), and 30.4 kJ mol^{-1} (right column). The color code is defined in Figure 3b. (c) LAB distributions recorded in the reaction of ground-state carbon atoms, $C(^3P_j)$, with D2-acetylene, $C_2D_2(X^1\Sigma_g^+)$ at $m/z = 38$ (C_3D^+) (upper row) and $m/z = 36$ (C_3^+) (lower row) for three collision energies at 8.0 (left column), 19.8 (central column), and 31.0 kJ mol^{-1} (right column). The color code is defined in Figure 3c. (d) LAB distributions recorded in the reaction of ground-state carbon atoms, $C(^3P_j)$, with D1-acetylene, $C_2HD(X^1\Sigma^+)$ at $m/z = 38$ (C_3D^+) (upper row), $m/z = 37$ (C_3H^+) (central row), and $m/z = 36$ (C_3^+) (lower row) for three collision energies at 8.1 kJ mol^{-1} (left column), 19.5 kJ mol^{-1} (central column), and 30.6 kJ mol^{-1} (right column). The color code is defined in Figure 3d.

compute R' , that is, the fraction of the molecular hydrogen elimination pathway to the sum of the atomic plus molecular hydrogen elimination pathway (eq 2).

$$R' = \frac{\sigma_{C_3}}{\sigma_{C_3H} + \sigma_{C_3}} = \frac{1}{R + 1} \quad (2)$$

The results are summarized in Figure 6. For each system studied, it is evident that the relative importance of the molecular versus atomic hydrogen/deuterium channel drops as the collision energy increases, that is, from 59–72% to only 21–38% at collision energies in the range of 8.0–8.1 kJ mol^{-1} and 30.4–31.0 kJ mol^{-1} , respectively. We would like to stress that because of the absence of $m/z = 38$ from elastically scattered $^{13}C_2^{12}C$ in case of the $C(^3P_j)^{13}C_2H_2(X^1\Sigma_g^+)$ reaction, the error bars are the lowest (about $\pm 5\%$) compared to $\pm 10\%$ in the remaining systems investigated. Also, the branching ratios derived for the $C(^3P_j)^{13}C_2H_2(X^1\Sigma_g^+)$ reaction are systematically lower than the other systems probed in the crossed beam studies.

In case of the $C(^3P_j)C_2HD(X^1\Sigma^+)$ system, we were also able to investigate the relative importance of the atomic hydrogen versus atomic deuterium elimination pathway. Here, reaction products were enriched in deuterium at both lower collision

energies of 8.1 kJ mol^{-1} and 19.5 kJ mol^{-1} yielding relative cross sections, $\sigma_{C_3D}/\sigma_{C_3H}$ of 1.55 ± 0.11 and 1.47 ± 0.19 , respectively. At the highest collision energy investigated, we could not find any deuterium enrichment within the error limits, that is, giving $\sigma_{C_3D}/\sigma_{C_3H} = 1.07 \pm 0.09$.

4. Discussion

4.1. The H/D Elimination Channel. We can compare now our experimental findings with the computed potential energy surfaces (Figure 1) and also in light of dynamics calculations.^{18–20} Considering the atomic hydrogen elimination pathway, the energy-dependent shape of the center-of-mass angular distributions of the $C(^3P_j)C_2H_2(X^1\Sigma_g^+)$, that is, an increasingly forward distribution as the collision energy drops (Figure 5), correlates nicely with our previous studies conducted with a pulsed carbon and continuous acetylene beam. This result alone confirms that in the present experiment the timing sequence of both the pulsed carbon and acetylene beams is correct. Recall that our previous studies on the hydrogen atomic elimination pathway suggested that at lower collision energies, the cyclic isomer was inferred to be formed through a triplet cyclopropenylidene intermediate (**12**) via direct scattering dynamics, that is, stripping of the C_2H unit from the acetylene to yield a cyclic C_3H molecule through

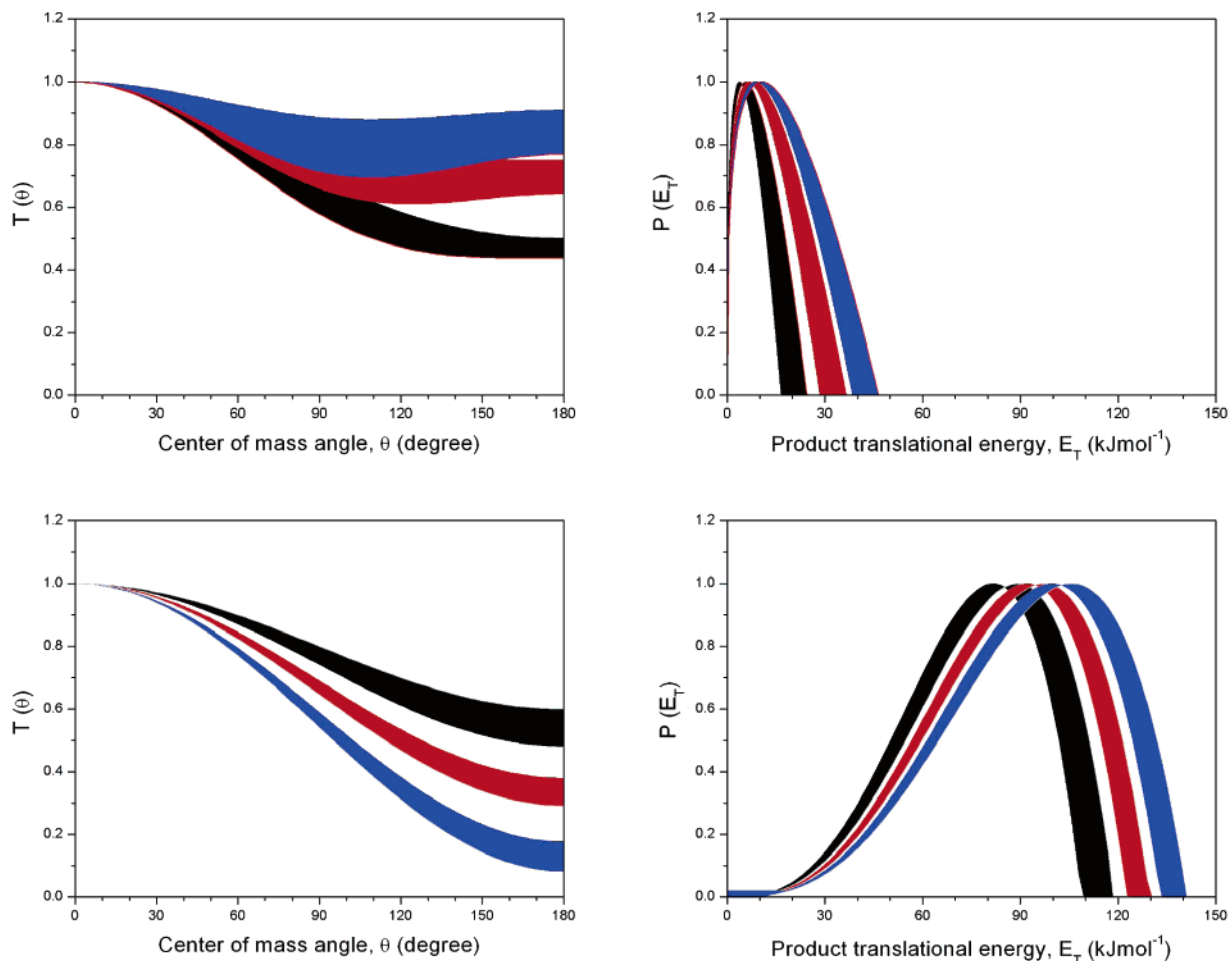


Figure 5. Center-of-mass angular (left column) and translational energy flux distributions (right column) for the tricarbon hydride (upper row) and tricarbon (lower row) reaction pathways carried out in three different ranges of collision energies at 8.0–8.1 kJ mol^{-1} (black), 19.3–20.4 kJ mol^{-1} (red), and 30.4–31.0 kJ mol^{-1} (blue). Regions of identical colors indicate the fits obtained within the error limits of our experiments.

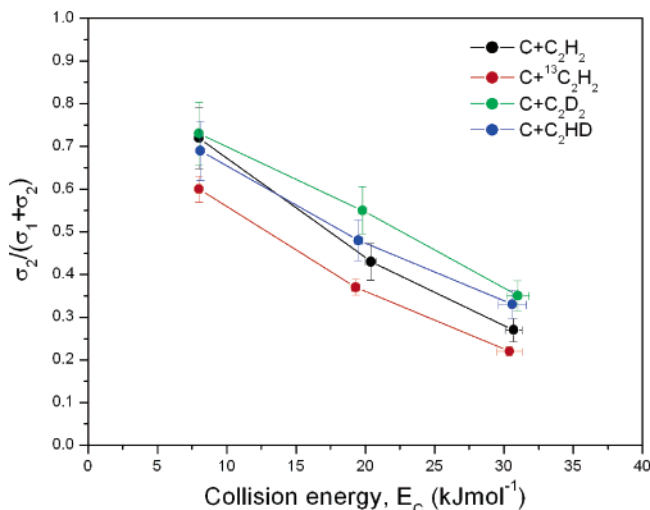


Figure 6. Branching ratios of the atomic hydrogen/deuterium (σ_1) versus the molecular hydrogen/deuterium/deuteriumhydride elimination pathways (σ_2) in the reaction of atomic carbon, $\text{C}(^3\text{P}_j)$, with acetylene and isotopically labeled acetylene reactants.

a short-lived triplet C_3H_2 intermediate (**t2**) (forward scattered microchannel); the linear C_3H isomer was inferred to be formed via a propargylene intermediate **t4** (Figure 1) (forward–backward symmetric microchannel); as the collision energy was raised, the relative contribution of the cyclic isomer compared to the linear structure decreased.^{11,12} The present isotopically

labeled experiments help to extract additional information on the scattering dynamics. The $\text{C}(^3\text{P}_j)\text{C}_2\text{HD}(X^1\Sigma^+)$ system can answer the question to what extent the forward–backward symmetry of the center-of-mass angular distribution of the microchannel leading via triplet propargylene (**t4**) to $l\text{-C}_3\text{H}$ is the result of a long-lived triplet propargylene intermediate or an artifact of the C_2 symmetry of intermediate (symmetric intermediate). By conducting the experiment with D1-acetylene, the symmetry of the D1-propargylene intermediate, DCCCH, reduces to C_1 . If the D1-propargylene intermediate is truly long-lived, we would not expect a change of shape in the center-of-mass laboratory angular distribution by switching from the acetylene to the D1-acetylene reactant.

However, if the forward–backward symmetry of the microchannel resulting from triplet propargylene is solely the result of the C_2 symmetry, we would expect that the center-of-mass laboratory angular distribution changes as we replace one hydrogen atom by deuterium. As a matter of fact, we were able to fit, at each collision energy, the $\text{C}(^3\text{P}_j)\text{C}_2\text{H}_2(X^1\Sigma_g^+)$, $\text{C}(^3\text{P}_j){}^{13}\text{C}_2\text{H}_2(X^1\Sigma_g^+)$, $\text{C}(^3\text{P}_j)\text{C}_2\text{HD}(X^1\Sigma^+)$, and $\text{C}(^3\text{P}_j)\text{C}_2\text{D}_2(X^1\Sigma_g^+)$ systems with identical center-of-mass angular distributions. Therefore, we can conclude that, at least in the range of 8–31 kJ mol^{-1} , the lifetime of the triplet propargylene intermediates is longer than the rotation period of the propargylene intermediate; on the basis of the $\text{C}(^3\text{P}_j)\text{C}_2\text{HD}(X^1\Sigma^+)$ experiments, the forward–backward symmetric microchannel leading to the linear tricarbon hydride isomer is clearly not an artifact of the C_2 symmetry of the propargylene and D1-

propargylene reaction intermediates. Likewise, we have to conclude that the ^{13}C -substituted propargylene intermediates formed in the reaction of $\text{C}(^3\text{P}_j)$ with $^{13}\text{C}_2\text{H}_2(\text{X}^1\Sigma_g^+)$ (Figure 2) are also most likely long-lived. Recall that the linear tricarbon hydride isomer can be formed via multiple reaction pathways (Figure 2). Most importantly, a hydrogen shift can interconvert both cyclopropenylidene isotopomers thus effectively scrambling the ^{13}C isotopes in the resulting propargylene isomer (**t4**).³¹ Future high-resolution spectroscopy of the reaction products should be able to identify three distinct isotopomers of the linear tricarbon hydride isomer (Figure 2).

We would like to comment briefly on the energetics of the reaction to emit atomic hydrogen/deuterium. Because of the light hydrogen/deuterium atom, the high-energy cutoffs are relatively insensitive to adding or cutting 5 kJ mol^{-1} to reaction energies. The experimentally obtained reaction energies of $20 \pm 5\text{ kJ mol}^{-1}$, recall that the center-of-mass translational energy distributions are quasi identical within the error limits for all the isotopically labeled reactants, agree reasonably well with the computed reaction energies to form the cyclic C_3H and the linear C_3H plus atomic hydrogen of $\Delta_R G = -8\text{ kJ mol}^{-1}$ and $\Delta_R G = -2\text{ kJ mol}^{-1}$,³² the authors quoted uncertainties of their calculations of $\pm 5\text{ kJ mol}^{-1}$. These energetics suggest that the cyclic isomer is certainly one of the reaction products.

It is also worthwhile commenting on the peak positions of the $P(E_T)$ s. If the reaction involves only a single reaction pathway passing through a triplet propargylene intermediate via indirect scattering dynamics, we would expect a simple bond rupture process to form the linear tricarbon hydride isomer plus atomic hydrogen/deuterium (Figure 1). This would be reflected in $P(E_T)$ s peaking at zero translational energy. This was clearly not observed (Figure 5). As a matter of fact, the observed off-zero peaking can be understood either in terms of a complex decomposing through a tight exit transition state or by a reaction in which one microchannel follows direct scattering dynamics.²⁹ On the basis of the PES (Figure 3), only triplet vinylidene carbene (**t3**) emits a hydrogen atom via a tight exit transition state located 31 kJ mol^{-1} above the separated reactants. However, at both lowest collision energies, this transition state is energetically not accessible in our experiments; we can therefore conclude that **t3** does not play a role in the scattering dynamics. This conclusion gains support from the PES involved. **t3** can only be formed via atomic hydrogen shift in **t1** through a barrier located about 64 kJ mol^{-1} above **t1**. However, investigating the barriers involved, **t1** rearranges preferentially via a hydrogen migration to **t4** (barrier: 2 kJ mol^{-1}) or by ring closure to form cyclopropenylidene (**t2**) (barrier: 3 kJ mol^{-1}). In this context, we should also realize that **t5** can likely be ruled out as an intermediate in the present reaction. A hydrogen migration in cyclopropenylidene (**t2**) presents the only pathway to form **t5**. However, the inherent barrier of 193 kJ mol^{-1} is likely too high to compete with the ring-opening process from **t2** to **t4** (barrier: 76 kJ mol^{-1}).

4.2. The $\text{H}_2/\text{D}_2/\text{HD}$ Elimination Channel. Our experiments present also comprehensive data on the molecular hydrogen elimination pathway. Recall that Mebel et al. suggested that the formation of the tricarbon molecule involves intersystem crossing (ISC) from triplet propargylene (**t4**) to singlet cyclopropenylidene (**s1**).¹⁵ The latter isomerizes through an atomic hydrogen migration to vinylidene carbene (**s2**), which loses molecular hydrogen (Figure 1). The present experiments confirm various aspects of this proposed mechanism. First, the center-of-mass angular distributions clearly indicate that the reaction dynamics are indirect (Figure 5). Second, the off-zero-peaking

TABLE 2: Moments of Inertia, I , and Estimated Life Time, τ , of the Vinylidene Carbene Intermediate at Various Collision Energies

	I_A (kg m ²)	I_B (kg m ²)	I_C (kg m ²)
H_2CCC	2.9×10^{-47}	7.9×10^{-46}	8.2×10^{-46}
	$\tau(A)$ (ps)	$\tau(B)$ (ps)	$\tau(C)$ (ps)
H_2CCC (8 kJ mol^{-1})	0.023 ± 0.003	0.57 ± 0.06	0.59 ± 0.08
H_2CCC (21 kJ mol^{-1})	0.009 ± 0.001	0.26 ± 0.03	0.27 ± 0.03
H_2CCC (31 kJ mol^{-1})	0.0040 ± 0.0004	0.12 ± 0.02	0.12 ± 0.02

of the $P(E_T)$ s at $85\text{--}110\text{ kJ mol}^{-1}$ suggests the existence of a tight exit transition state leading to the formation of molecular hydrogen. Indeed, the computations confirm an exit barrier of about 100 kJ mol^{-1} to form tricarbon plus molecular hydrogen. This is also supported by the large fraction of energy channeling into the translational degrees of freedom, that is, $66 \pm 6\%$ independent of the collision energy (section 3.2). This data compares well with Costes et al. deriving fractions between 50% and 66%.³³ Third, the energy-dependent change in the center-of-mass angular distributions, that is, an enhanced forward scattering as the collision energy rises, indicates the existence of one osculating C_3H_2 complex leading to tricarbon plus molecular hydrogen.²⁸ We can utilize the $T(0^\circ)/T(180^\circ)$ ratio (section 3.2) to estimate the lifetime of the singlet vinylidene carbene intermediate. Here, the osculating model relates the intensity ratio of $T(\theta)$ at both poles to τ via eq 3

$$I(180^\circ)/I(0^\circ) = \exp\left(-\frac{t_{\text{rot}}}{2\tau}\right) \quad (3)$$

where t_{rot} represents the rotational period with

$$t_{\text{rot}} = 2\pi I_i/L_{\text{max}} \quad (4)$$

I_i stands for the moment of inertia of the complex rotating around the i -axis ($i = A, B, C$), and L_{max} stands for the maximum orbital angular momentum. Using the moments of inertia of the vinylidene carbene intermediate (**s2**)¹⁵ and taking the maximum impact parameter to be in the order of 3.6, 2.8, and 2.6 Å at collision energies of 8, 21, and 31 kJ mol^{-1} ,^{11,34} the reduced mass of the reactants of $8.2 \times 10^{-3}\text{ kg mol}^{-1}$, and the relative velocity of the reactants as computed from Table 1, we obtain maxima orbital angular momenta of 6.8×10^{-33} , 8.6×10^{-33} , and $9.7 \times 10^{-33}\text{ kg m}^2\text{ s}^{-1}$ from the lowest to the highest collision energy. Employing the rotational constants from Mebel et al.,¹⁵ we can calculate the lifetime of the vinylidene carbene intermediates as compiled in Table 2. Recalling that reactions with collision times $\ll 0.1\text{ ps}$ go hand in hand with direct scattering dynamics,³⁴ the $T(\theta)$ s should be strongly forward scattered; this was clearly not observed experimentally. Therefore, we can conclude that the vinylidene carbene intermediates cannot rotate around the A axes but are rather excited to B/C like rotations prior to decomposition via molecular hydrogen loss to form tricarbon molecule. We find that as the collision energy increases, the lifetime of the vinylidene carbene (**s2**) intermediate, which is excited to B/C like rotations, decreases from 0.57 to 0.12 ps.

The increased collision energy is also expected to go hand in hand with a reduced intersystem crossing rate constant and, hence, with a diminished branching ratio of the molecular hydrogen loss channel. Our experiments clearly verify this predicted trend (Figure 4). Considering the $\text{C}(^3\text{P}_j)\text{C}_2\text{H}_2(\text{X}^1\Sigma_g^+)$ system, the branching ratio of the molecular hydrogen elimination channel drops from $73 \pm 7\%$ via $42 \pm 5\%$ to $29 \pm 3\%$.

Balucani and co-workers reported a similar tendency in the range of 3.5–29.3 kJ mol⁻¹.^{33,35} At the highest collision energy, they report a branching ratio of 37%; since the authors do not provide error limits, we cannot present a quantitative comparison of both experiments. We also would like to comment briefly on the molecular elimination channel in the C(³P_j)C₂HD(X¹Σ⁺) and C(³P_j)C₂D₂(X¹Σ_g⁺) systems. First, the branching ratios of the HD loss pathway in the C₂HD(X¹Σ⁺) reaction is similar to the molecular hydrogen loss in the C(³P_j)C₂H₂(X¹Σ_g⁺) system. However, the molecular deuterium loss channel in the C(³P_j)C₂D₂(X¹Σ_g⁺) reactions is, at all three collision energies, systematically larger than the corresponding molecular hydrogen loss pathways. Can this be simply an effect of the enhanced mass of the D₂-acetylene compared to the acetylene reactant? Comparing the C(³P_j)C₂D₂(X¹Σ_g⁺) with the C(³P_j)¹³C₂H₂(X¹Σ_g⁺) system, we see that despite an identical mass of the isotopically substituted intermediates the branching ratios for the D₂ loss is higher than for the H₂ loss. Also, the symmetry of the reaction intermediates in the C(³P_j)C₂D₂(X¹Σ_g⁺) and C(³P_j)¹³C₂H₂(X¹Σ_g⁺) reactions can influence the spin-orbit coupling matrix element. Here, intersystem crossing (ISC) occurs since the spin-orbit coupling operator acts as a perturbation capable of mixing the triplet wave function (³B in propargylene) with the final singlet wave function (¹A in cyclopropenylidene; reduced via C₂ symmetry). Since the operators transform as rotations, they span the irreducible representations A, B, and B. Hence, the ³B state of propargylene is mixed via a B spin-orbit operator with the ¹A state of cyclopropenylidene. In the C(³P_j)¹³C₂H₂(X¹Σ_g⁺) system, this consideration also holds if the ¹²C atom is in the center of the propargylene intermediate. However, if the ¹²C is connected to a hydrogen atom, the symmetry of the isotopically labeled propargylene intermediate is reduced from C₂ to C₁. Under the C₁ point group, the components of the spin-orbit operators hold A, A, and A symmetries. Current theoretical calculations are on the way to investigate these effects quantitatively.³⁶ The C(³P_j)¹³C₂H₂(X¹Σ_g⁺) reaction is also expected to form two isotopomers of tricarbon: ¹²C–¹³C–¹³C and ¹³C–¹²C–¹²C via two distinct propargylene intermediates through ISC to two vinylidene carbene isotopomers (Figure 2). The reaction to form cyclic tricarbon, C₃(X³A₂') plus molecular hydrogen, is exoergic by 42 kJ mol⁻¹ (Figure 1).³⁷ However, the barrier to molecular hydrogen elimination is about 200 kJ mol⁻¹ which makes this reaction pathway energetically not accessible.²¹

Finally, it is valuable to mention that the atomic hydrogen loss pathway may also originate from the singlet surface. For instance, the intermediates **s1** and **s2** can emit atomic hydrogen to form the cyclic and linear C₃H isomers, respectively. Recent dynamics calculations support this statement indicating that on the singlet surface, tricarbon, linear C₃H, and cyclic C₃H are formed with almost equal branching ratios.²¹ A combination of our experimentally derived branching ratios for the molecular versus atomic hydrogen loss channels (and their isotopic analogues) and also the H/D loss branching ratios in the C(³P_j)C₂HD(X¹Σ⁺) system with future dynamics and statistical calculations will shed light on the open question to what extent the triplet and singlet surfaces are involved in this reaction.

6. Summary and Conclusions

We investigated the multichannel reaction of ground-state carbon atoms with acetylene, C₂H₂ (X¹Σ_g⁺), to form the linear and cyclic C₃H isomers (atomic hydrogen elimination pathway) as well as tricarbon plus molecular hydrogen. The experiments were conducted under single-collision conditions at three different collision energies between 8.0 kJ mol⁻¹ and 31.0 kJ

mol⁻¹. Our studies were complemented for the first time by crossed molecular beam experiments of carbon with three isotopomers C₂D₂(X¹Σ_g⁺), C₂HD(X¹Σ⁺), and ¹³C₂H₂(X¹Σ_g⁺) to clarify a potential intersystem crossing (ISC), the effect of the symmetry of the reaction intermediates on the center-of-mass angular distributions, the collision-energy-dependent branching ratios of the atomic versus molecular elimination pathways, and potential deuterium enrichment processes. We could provide for the first time branching ratios over a wide range of collision energies. Here, as the collision energy increases, the molecular hydrogen elimination pathways become less important; the corresponding branching ratios were found to decrease from about 73 ± 7% via 42 ± 5% to 29 ± 3%. This is in line with decreasing intersystem crossing rate constants as the collision energy is raised. Simultaneously, we found that the lifetime of the decomposing singlet vinylidene carbene decreases from about 0.57 ps at the lowest to only 0.12 ps at the highest collision energy investigated. Second, we detected a dependence of the branching ratios at similar collision energies on the nature of the isotopically labeled reactants, that is, substituting ¹²C by ¹³C and one/two H atoms by one/two D atoms. In addition to the molecular hydrogen elimination pathway, we also obtained valuable information of the properties of triplet propargylene and its isotopomers. Our experiments reveal that the propargylene intermediate is truly long-lived and that the forward-backward symmetry of the microchannel leading to the linear C₃H isomer is not the artifact of the C₂ symmetry of the reaction intermediate. Finally, we proposed the existence of several ¹³C-substituted linear tricarbon hydride and tricarbon isotopomers which could be probed in future spectroscopic investigation of this reaction.

Acknowledgment. This work was supported by the U.S. National Science Foundation (CHE-0234461). We would also thank Ed Kawamura (UH Chemistry) for support.

References and Notes

- (1) Minh, Y. C.; van Dishoeck, E. F. *Astrochemistry: From Molecular Clouds to Planetary Systems*; Astronomical Society of the Pacific: San Francisco, CA, 2000.
- (2) Lis, D. C.; Blake, G. A.; Herbst, E. *Astrochemistry: Recent successes and current challenges*; Cambridge University press, 2006.
- (3) Shaw, A. M. *Astrochemistry from astronomy to astrobiology*; John Wiley & Sons Ltd.: West Sussex, U.K., 2006.
- (4) Kaiser, R. I.; Ochsenfeld, C.; Stranges, D.; Head-Gordon, M.; Lee, Y. T. *Faraday Discuss.* **1998**, *109*, 183.
- (5) Faraday Discussion 119, Combustion Chemistry: Elementary Reactions to Macroscopic Processes 2001.
- (6) Frenklach, M. *Phys. Chem. Chem. Phys.* **2002**, *4*, 2028.
- (7) Nienow, A. M.; Roberts, J. T. *Annu. Rev. Phys. Chem.* **2006**, *57*, 4.
- (8) Clary, D. C.; Haider, N.; Husain, D.; Kabir, M. *Astrophys. J.* **1994**, *422*, 416. Haider, N.; Husain, D. *J. Chem. Soc., Faraday Trans.* **1993**, *89*, 7.
- (9) Chastaing, D.; James, P. L.; Sims, I. R.; Smith, I. W. M. *Phys. Chem. Chem. Phys.* **1999**, *1*, 2247. Chastaing, D.; Le Picard, S. D.; Sims, I. R.; Smith, I. W. M. *Astron. Astrophys.* **2001**, *365*, 241.
- (10) Kaiser, R. I.; Lee, Y. T.; Suits, A. G. *J. Chem. Phys.* **1995**, *103*, 10395.
- (11) Kaiser, R. I.; Lee, Y. T.; Suits, A. G. *J. Chem. Phys.* **1996**, *105*, 8705.
- (12) Kaiser, R. I.; Ochsenfeld, C.; Head-Gordon, M.; Lee, Y. T.; Suits, A. G. *Science* **1996**, *274*, 1508.
- (13) Kaiser, R. I.; Le, T. N.; Nguyen, T. L.; Mebel, A. M.; Balucani, N.; Lee, Y. T.; Stahl, F.; Schleyer, P. V. R.; Schaefer, H. F., III. *Faraday Discuss.* **2001**, *119*, 51.
- (14) Casavecchia, P.; Balucani, N.; Cartechini, L.; Capozza, G.; Bergeat, A.; Volpi, G. G. *Faraday Discuss.* **2001**, *119*, 27. Costes, M.; Daugey, N.; Naulin, C.; Bergeat, A.; Leonori, F.; Segoloni, E.; Petrucci, R.; Balucani, N.; Casavecchia, P. *Faraday Discuss.* **2005**, *133*, 1.

- (15) Mebel, A. M.; Jackson, W. M.; Chang, A. H. H.; Lin, S. H. *J. Am. Chem. Soc.* **1998**, *120*, 5751.
- (16) Geppert, W. D.; Naulin, C.; Costes, M. *Chem. Phys. Lett.* **2001**, *333*, 51. Clay, D. C.; Buonomo, E.; Sims, I. R.; Smith, I. W. M.; Geppert, W. D.; Naulin, C.; Costes, M.; Cartechini, L.; Casavecchia, P. *J. Phys. Chem. A* **2002**, *106*, 5541.
- (17) Bergeat, A.; Loison, J.-C. *Phys. Chem. Chem. Phys.* **2001**, *3*, 2038.
- (18) Ochsenfeld, C.; Kaiser, R. I.; Lee, Y. T.; Suits, A. G.; Head-Gordon, M. *J. Chem. Phys.* **1997**, *106*, 414. Takahashi, J.; Yashimata, K. *J. Chem. Phys.* **1996**, *104*, 6613. Guadagnini, R.; Schatz, G. C.; Walch, S. P. *J. Phys. Chem. A* **1998**, *102*, 5857. Mebel, A. M.; Jackson, W. M.; Chang, A. H. H.; Lin, S. H. *J. Am. Chem. Soc.* **1998**, *120*, 5751. Buonomo, E.; Clary, D. C. *J. Phys. Chem. A* **2001**, *105*, 2694.
- (19) Buonomo, E.; Clary, D. C. *J. Phys. Chem. A* **2001**, *105*, 2694.
- (20) Takayanagi, T. *J. Phys. Chem. A* **2006**, *110*, 361.
- (21) Park, W. K.; Park, J.; Park, S. C.; Braams, B. J.; Chen, C.; Bowman, J. M. *J. Chem. Phys.* **2006**, *125*, 081101.
- (22) Guo, Y.; Gu, X.; Kaiser, R. I. *Int. J. Mass Spectrom.* **2006**, *420*, 249–250. Gu, X.; Guo, Y.; Kaiser, R. I. *Int. J. Mass Spectrom.* **2005**, *246*, 29. Gu, X.; Guo, Y.; Kawamura, E.; Kaiser, R. I. *Rev. Sci. Instrum.* **2005**, *76*, 083115. Guo, Y.; Gu, X.; Kawamura, E.; Kaiser, R. I. *Rev. Sci. Instrum.* **2006**, *77*, 034701.
- (23) Gu, X.; Guo, Y.; Kawamura, E.; Kaiser, R. I. *J. Vac. Sci. Technol., A* **2006**, *24*, 505.
- (24) Gu, X.; Guo, Y.; Mebel, A. M.; Kaiser, R. I. *J. Phys. Chem. A* **2006**, *110*, 11265.
- (25) Kaiser, R. I.; Mebel, A. M.; Balucani, N.; Lee, Y. T.; Stahl, F.; Schleyer, P. v. R.; Schaefer, H. F. *Faraday Discuss.* **2001**, *119*, 51.
- (26) Weis, M. S. Ph.D. Thesis, University of California, Berkeley, 1986.
- (27) Vernon, M. Thesis, University of California, Berkeley, 1981.
- (28) Miller, W. B.; Safron, S. A.; Herschbach, D. R. *Discuss. Faraday Soc.* **1967**, *44*, 108.
- (29) Kaiser, R. I.; Mebel, A. M. *Int. Rev. Phys. Chem.* **2002**, *21*, 307.
- (30) Schmoltner A. M. Thesis, University of California, Berkeley, 1989.
- (31) Seburg, R. A.; Patterson, J. F.; Stanton, J. F.; McMahon, R. J. *J. Am. Chem. Soc.* **1997**, *119*, 5847.
- (32) Kaiser, R. I.; Ochsenfeld, C.; Head-Gordon, M.; Lee, Y. T. *Astrophys. J.* **1999**, *510*, 784.
- (33) Costes, M.; Daugey, N.; Naulin, C.; Bergeat, A.; Leonori, F.; Segoloni, E.; Petrucci, R.; Balucani, N.; Casavecchia, P. *Faraday Discuss.* **2006**, *133*, 157.
- (34) Levine, R. D. *Molecular Reaction Dynamics*; Cambridge University Press: Cambridge, U.K., 2005.
- (35) Balucani, N.; Capozza, G.; Leonori, F.; Segoloni, E.; Casavecchia, P. *Int. Rev. Phys. Chem.* **2006**, *25*, 109.
- (36) Mebel, A. M. Private communication, 2006.
- (37) Mebel, A. M.; Kaiser, R. I. *Chem. Phys. Lett.* **2002**, *360*, 136.